Stable Ordered FePt Mesoporous Silica Catalysts with High Loadings

Gaurav Gupta, Mehul N. Patel, Domingo Ferrer, Andrew T. Heitsch, Brian A. Korgel, Miguel Jose-Yacaman, and Keith P. Johnston*

Department of Chemical Engineering and Texas Materials Institute, Center for Nano- and Molecular Science and Technology, The University of Texas, Austin, Texas 78712-1062

A new concept is presented to form catalysts by infusion of presynthesized bimetallic nanocrystals into ordered mesoporous supports. For presynthesized FePt nanocrystals (<4 nm) coated with oleic acid and oleylamine ligands in toluene, high loadings above 10 wt % were achieved in 10 min. The strong metal−support interactions were favored by the low coverage of the weakly bound ligands. The nanocrystals were highly dispersed within the pores as indicated by HAADF-STEM and X-ray diffraction (XRD) and stable against sintering at 700 °C and desorption into polar and nonpolar solvents at room temperature. A phase transformation from a disordered phase (FCC) to ordered phase (FCT) was observed upon thermal annealing at 700 °C without sintering, as confirmed by convergent beam electron diffraction and XRD. The calcined FePt catalyst exhibited 6-fold higher catalyst activity (TOF = 30 s^{-1}) than that of a commercial Pd-alumina catalyst for liquid 1-decene hydrogenation and was stable for multiple reactions. The decoupling of nanocrystal synthesis and infusion provides exquisite control of the nanocrystal size, alloy structure, binding to the support and dispersibility within the pores, offering broad opportunities for enhanced catalyst activities, selectivities, and stabilities.

Introduction

Highly active and stable catalysts may be designed by controlling the size and composition of supported metal nanoparticles.[1–8] For supported catalysts synthesized by precursor reduction,[9,10] chemical vapor/fluid deposition,[11] or coprecipitation,[5,12] it is difficult to control the size and surface morphology of the metal clusters as well as the binding to the surface. An emerging concept in catalyst design is to presynthesize metal nanocrystals coated with stabilizing ligands to control the morphology and then infuse the particles onto high surface area ordered mesoporous supports.[13–15] The highly uniform and tunable size and curvature of 1D and 3D pores in ordered mesoporous substrates[16] facilitates dispersion and stability of the nanoparticles.[17–21]

The metal loading of catalysts formed with presynthesized nanocrystals has been found to be highly dependent on the stabilizing ligands on the particle surface. Infusion of Pt nanocrystals coated with polyvinylpyrollidone (PVP) ligands into mesoporous silica with sonication yielded a metal loading of approximately 1 wt %.[13] Gold[14] nanocrystals capped with dodecanethiol and iridium[22] with tetraoctylammonium bromide were loaded into mesoporous silica up to 2.5 wt %. The low-molecular-weight ligands facilitated ligand removal. The high catalytic activity for 1-decene hydrogenation without calcination suggests that the weakly bound ligand tetraoctylammonium bromide did not cover the

* Corresponding author. Fax: 512-471-7060. Phone: 512-471-4617. E-mail: kpj@che.utexas.edu.

(1) Fu, Q.; Saltsburg, H.; Flytzani-Stephanopoulos, M. *Science* **2003**, *301*, 935–938.
(2) Chen, M. S.; Goodman, D. W. *Science* **2004**, *306*, 252–255.
(3) Somorjai, G. A.; Contreras, A. M.; Montano, M.; Rioux, R. M. *Proc. Natl. Acad. Sci. U.S.A.* **2006**, *103*, 10577–10583.
(4) Akita, T.; Okumura, M.; Tanaka, K.; Kohyama, M.; Haruta, M. *Catal. Today* **2006**, *117*, 62–68.
(5) Meunier, F. C.; Tibiletti, D.; Goguet, A.; Shekhtman, S.; Hardacre, C.; Burch, R. *Catal. Today* **2007**, *126*, 143–147.
(6) Stamenkovic, V. R.; Mun, B. S.; Arenz, M.; Mayrhofer, K. J. J.; Lucas, C. A.; Wang, G.; Ross, P. N.; Markovic, N. M. *Nat. Mater.* **2007**, *6*, 241–247.
(7) Zheng, N.; Stucky, G. D. *J. Am. Chem. Soc.* **2006**, *128*, 14278–14280.
(8) Kang, S.; Jia, Z.; Zoto, I.; Reed, D.; Nikles, D. E.; Harrell, J. W.; Thompson, G.; Mankey, G.; Krishnamurthy, V. V.; Porcar, L. *J. Appl. Phys.* **2006**, *99*. 08N704/701−708N704/703.
(9) Wakayama, H.; Setoyama, N.; Fukushima, Y. *Adv. Mater.* **2003**, *15*, 742–745.
(10) Koh, S.; Toney, M. F.; Strasser, P. *Electrochim. Acta* **2007**, *52*, 2765–2774.
(11) Song, Z.; Cai, T.; Hanson, J. C.; Rodriguez, J. A.; Hrbek, J. *J. Am. Chem. Soc.* **2004**, *126*, 8576–8584.
(12) Li, Y.; Fu, Q.; Flytzani-Stephanopoulos, M. *Appl. Catal., B* **2000**, *27*, 179–191.
(13) Rioux, R. M.; Song, H.; Hoefelmeyer, J. D.; Yang, P.; Somorjai, G. A. *J. Phys. Chem. B* **2005**, *109*, 2192–2202.
(14) Gupta, G.; Shah, P. S.; Zhang, X.; Saunders, A. E.; Korgel, B. A.; Johnston, K. P. *Chem. Mater.* **2005**, *17*, 6728–6738.
(15) Tsung, C.-K.; Hong, W.; Shi, Q.; Kou, X.; Yeung, M. H.; Wang, J.; Stucky, G. D. *Adv. Funct. Mater.* **2006**, *16*, 2225–2230.
(16) Lee, J.; Kim, J.; Hyeon, T. *Adv. Mater.* **2006**, *18*, 2073–2094.
(17) Morey, M. S.; Davidson, A.; Stucky, G. D. *J. Porous Mater.* **1998**, *5*, 195–204.
(18) Hanrahan, J. P.; Copley, M. P.; Ziegler, K. J.; Spalding, T. R.; Morris, M. A.; Steytler, D. C.; Heenan, R. K.; Schweins, R.; Holmes, J. D. *Langmuir* **2005**, *21*, 4163–4167.
(19) Fan, J.; Boettcher, S. W.; Stucky, G. D. *Chem. Mater.* **2006**, *18*, 6391–6396.
(20) Zhao, D.; Feng, J.; Huo, Q.; Melosh, N.; Frederickson, G. H.; Chmelka, B. F.; Stucky, G. D. *Science* **1998**, *279*, 548–552.
(21) Joo, S. H.; Choi, S. J.; Oh, I.; Kwak, J.; Liu, Z.; Terasaki, O.; Ryoo, R. *Nature* **2001**, *412*, 169–172.
(22) Gupta, G.; Stowell, C. A.; Patel, M. N.; Gao, X.; Yacaman, M. J.; Korgel, B. A.; Johnston, K. P. *Chem. Mater.* **2006**, *18*, 6239–6249.

active sites. Recently, Jung et al.[23] showed that FePt nanocrystals could be infused in hydrophobic mesoporous silica, although the metal loading was not given. An alternative approach is to synthesize the mesoporous support in the presence of a nanocrystal dispersion.[24,25] However, the presence of the nanocrystals can interfere with the mesopore structure and conversely, the synthesis of the mesoporous material can alter the morphology and surface composition of the nanocrystals. To date, high metal loadings >10 wt % have received little attention for the infusion technique, but would be of interest in various applications.[6,26]

Multimetallic alloy nanocrystals often enable enhanced catalyst activities as a consequence of synergistic interactions between atoms,[27,28] including formation of ordered intermetallic nanocrystals.[6,28,29] The high annealing temperatures required to form these intermetallic alloys often leads to particle sintering.[30–32] Traditionally, bimetallic nanocrystals have been synthesized by reduction of multiple precursors over a metal support[30] or by decomposition of multimetal carbonyl precursors.[33] Thomas and co-workers decomposed specially synthesized multimetal carbonyl precursors thermally over mesoporous silica to form nanoclusters[27,34] composed of 10–20 atoms with a size of ~1 nm. Although these catalysts have great potential, larger metal nanocrystals ≥3 nm are in some cases more catalytically active than small metal clusters.[35]

The reduction of multiple metal precursors within porous supports often produces, high polydispersity and high variability in particle composition.[36] Without the use of stabilizing ligands, the nanocrystal size may exceed 10 nm and even reach the size of the pores of the support, as has been observed for FePt,[32] NiFe,[30] and PtCo[37] in mesoporous silica. For example, FePt nanoparticles grew to a size of 6 nm in mesoporous silica with 9 nm pores.[32] Here the nanoparticles may block some of the pores. The varying rates of nucleation and growth for each metal precursor over the heterogeneous sites on the supports may lead to highly variable composition.[36] For example, the composition varied for Pt:Co between 44:56 and 97:3, and the size reached 6–10 nm.[37] Potentially, these limitations may be overcome by infusion of presynthesized bimetallic nanocrystals into the porous support, although this approach has received little attention. For example, FePt nanocrystals have been synthesized with precise control over the nanocrystal size, shape, and composition by arrested growth precipitation.[38–41]

The primary objectives of this study were to: (1) design active and stable catalysts at high loadings above 10 wt % by infusion of presynthesized FePt nanocrystals on mesoporous silica and (2) to transform the crystal structure to a face centered tetragonal (FCT) intermetallic alloy upon annealing at 700 °C without perturbing the size. These objectives were facilitated by designing stabilizing ligands to strengthen short-ranged interactions between bare Pt and silica, which have been characterized by XPS,[42] EELS,[43] and wettability studies[44] at high temperatures. Because various types of ligands such as dodecanethiol[14] and polyvinylpyrrolidone[13] screen these interactions, we chose to investigate weakly bound oleic acid and oleylamine low-molecular-weight ligands that expose a greater fraction of the metal surface domains. The large interfacial area between the spherical nanocrystals and concave mesopores with similar diameters favors nanocrystal–support interactions, relative to other support geometries.

The size and composition of the nanocrystals was determined by X-ray diffraction and high angle annular dark field-scanning transmission electron microscopy (HAADF-STEM). The kinetics and equilibrium loading of nanocrystals in mesoporous silica were studied as a function of the initial nanocrystal concentration over a period from 10 min to 16 h. The nanocrystals within the pores were differentiated from those on the external silica surface by HAADF-STEM. Finally, the catalyst activity and stability for liquid phase hydrogenation of 1-decene were examined both before and after calcination.

Experimental Section

All chemicals were used as received. Platinum(II) acetylacetonate (97%), iron(0) pentacarbonyl (99.999%), oleylamine (70%), oleic acid (99%), and 1,2 hexadecanediol (90%) were purchased from Aldrich. Toluene (99. 9%) and concentrated liquid HCl (normality 12.1) were obtained from Fisher Scientific, and ethanol (Absolute 200 proof) from Aaper alcohol. Tetraethoxysilane (TEOS) and dioctylether (97%) were obtained from Fluka Chemika. Poly(ethylene oxide)-*b*-poly(propylene oxide)-*b*-poly(ethylene oxide)

(23) Jung, J. S.; Lim, J. H.; Malkinski, L.; Vovk, A.; Choi, K. H.; Oh, S. L.; Kim, Y. R.; Jun, J. H. *J. Magn. Magn. Mater.* **2007**, *310*, 2361–2363.

(24) Konya, Z.; Puntes, V. F.; Kiricsi, I.; Zhu, J.; Ager, J. W., III; Ko, M. K.; Frei, H.; Alivisatos, P.; Somorjai, G. A. *Chem. Mater.* **2003**, *15*, 1242–1248.

(25) Song, H.; Rioux, R. M.; Hoefelmeyer, J. D.; Komor, R.; Niesz, K.; Grass, M.; Yang, P.; Somorjai, G. A. *J. Am. Chem. Soc.* **2006**, *128*, 3027–3037.

(26) Raghuveer, V.; Manthiram, A.; Bard, A. J. *J. Phys. Chem. B* **2005**, *109*, 22909–22912.

(27) Raja, R.; Khimyak, T.; Thomas, J. M.; Hermans, S.; Johnson, B. F. G. *Angew. Chem., Int. Ed.* **2001**, *40*, 4638–4642.

(28) Casado-Rivera, E.; Volpe, D. J.; Alden, L.; Lind, C.; Downie, C.; Vazquez-Alvarez, T.; Angelo, A. C. D.; DiSalvo, F. J.; Abruna, H. D. *J. Am. Chem. Soc.* **2004**, *126*, 4043–4049.

(29) Xu, Y.; Ruban, A. V.; Mavrikakis, M. *J. Am. Chem. Soc.* **2004**, *126*, 4717–4725.

(30) Folch, B.; Larionova, J.; Guari, Y.; Datas, L.; Guerin, C. *J. Mater. Chem.* **2006**, *16*, 4435–4442.

(31) Vondrova, M.; Klimczuk, T.; Miller, V. L.; Kirby, B. W.; Yao, N.; Cava, R. J.; Bocarsly, A. B. *Chem. Mater.* **2005**, *17*, 6216–6218.

(32) Kockrick, E.; Krawiec, P.; Schnelle, W.; Geiger, D.; Schappacher, F. M.; Poettgen, R.; Kaskel, S. *Adv. Mater.* **2007**, *19*, 3021–3026.

(33) Hermans, S.; Raja, R.; Thomas, J. M.; Johnson, B. F. G.; Sankar, G.; Gleeson, D. *Angew. Chem., Int. Ed.* **2001**, *40*, 1211–1215.

(34) Thomas, J. M.; Johnson, B. F. G.; Raja, R.; Sankar, G.; Midgley, P. A. *Acc. Chem. Res.* **2003**, *36*, 20–30.

(35) Valden, M.; Lai, X.; Goodman, D. W. *Science* **1998**, *281*, 1647–1650.

(36) Zhou, B.; Hermans, S.; Somorjai, G. A. *Nanotechnology in Catalysis*; Kluwer Academic/Plenum: New York, 2004; Vol. 1.

(37) King, N. C.; Blackley, R. A.; Wears, M. L.; Newman, D. M.; Zhou, W.; Bruce, D. W. *Chem. Commun.* **2006**, 3414–3416.

(38) Sun, S.; Murray, C. B.; Weller, D.; Folks, L.; Moser, A. *Science* **2000**, *287*, 1989–1992.

(39) Chen, M.; Liu, J. P.; Sun, S. *J. Am. Chem. Soc.* **2004**, *126*, 8394–8395.

(40) Sun, S.; Fullerton, E. E.; Weller, D.; Murray, C. B. *IEEE Trans. Magn.* **2001**, *37*, 1239–1243.

(41) Chen, M.; Kim, J.; Liu, J. P.; Fan, H.; Sun, S. *J. Am. Chem. Soc.* **2006**, *128*, 7132–7133.

(42) Komiyama, M.; Shimaguchi, T. *Surf. Interface Anal.* **2001**, *32*, 189–192.

(43) Klie, R. F.; Disko, M. M.; Browning, N. D. *J. Catal.* **2002**, *205*, 1–6.

(44) Yu, R.; Song, H.; Zhang, X.-F.; Yang, P. *J. Phys. Chem. B* **2005**, *109*, 6940–6943.

EÕ$_{20}$PÕ$_{70}$EÕ$_{20}$ (Pluronic P123) was obtained from BASF Corporation. Polycarbonate filters (0.05 μm) were obtained from Osmonics. Water was doubly distilled and deionized.

FePt Nanocrystal Synthesis. 3−4 nm spherical FePt nanocrystals were synthesized with the high temperature arrested precipitation method developed be Sun et al.[38] The reaction was carried out under a N$_2$ environment with a Schlenk Line. The nanocrystals were prepared by mixing 0.098 g (0.25 mmol) platinum(II) acetylacetonate, 0.195 g (0.77 mmol) 1,2-hexadecanediol, and 10 mL of dioctyl ether in a 50 mL three-neck flask. The stirred solution was heated to 100 °C under N$_2$ flow, and 0.065 mL (0.50 mmol) of iron(0) pentacarbonyl, 0.085 mL (0.26 mmol) of oleylamine, and 0.08 mL (0.25 mmol) of oleic acid were injected. The temperature was raised at a rate of 20 °C/min to the reflux temperature of dioctyl ether (297 °C) and the reaction solution was incubated for 30 min. The solution was allowed to cool to room temperature and excess ethanol was used to precipitate the FePt nanocrystals, which were recovered after centrifugation (10 min, 8000 rpm). The nanocrystals were washed twice by redispersing them in hexane and repeating the precipitation procedure. No additional size-selective precipitation was necessary to obtain the monodispersity.

Mesoporous Silica Synthesis. Mesoporous silica SBA-15 was synthesized with a block copolymer template with the exact procedure of Zhao et al.[20,45] A solution of 1.6 g EO$_{20}$PO$_{70}$EO$_{20}$:7 mL HCl:8 mL TEOS:38 mL H$_2$O was prepared, stirred for 24 h at 50 °C, and then heated at 100 °C for 24 h. The resulting slightly yellow powder was dispersed in ethanol, filtered, and then again heated at 100 °C for 24 h. Calcination was carried out by slowly increasing the temperature from room temperature to 550 °C in 4 h and heating at 550 °C for 6 h.

Infusion of FePt into Mesoporous Silica and Nanocomposite Stability. To prepare the supported nanocrystal composites, we mixed 10 mg of mesoporous silica with 3 mL of FePt nanocrystal dispersion in toluene of known concentrations from 0.25 to 2 mg/mL. The contents were then stirred for ∼10 min. After stirring, the mesoporous silica infused with FePt nanocrystals was separated from the nanocrystal supernatant by filtration with a 0.2 μm PTFE filter. The extent of incorporation of FePt nanocrystals in the silica was determined by subtracting from the initial mass of the dispersed nanocrystals in toluene, the final mass of the nanocrystals recovered in the supernatant after filtration.[14] The absorbance of the FePt nanocrystals dispersed in toluene before and after infusion was measured at a wavelength of 500 nm using a Cary 500 UV−vis−NIR spectrophotometer with an optical path length of 1 cm. A standard calibration curve was generated with known concentrations of FePt nanocrystals in toluene as shown in the Supporting Information (Figure S1). The experiments were repeated three times to check for the reproducibility in the nanocrystal loading, which was on the order of ±0.2 in wt % unit. Total uncertainty in loadings determined with this technique was approximately 12% as explained in detail previously.[22] The uncertainty for this method is comparable to that for elemental analysis (10% error). The stability of the nanocrystals immobilized within the pores was studied by suspending the nanocomposite in pure ethanol. The suspension was sonicated for 2 h after which the nanocomposite was separated by vacuum filtration, redispersed in ethanol, and analyzed by using UV−vis spectroscopy.

Calcination. To modify the crystal structure of FePt, we calcined nanocomposites at 700 °C in a N$_2$/H$_2$ atmosphere for 4 h. Temperature was ramped from ambient to 700 °C in 20 min. To activate the FePt for catalysis, nanocomposites were calcined in

stagnant air at 500 °C for 4 h. Temperature was ramped from ambient to 500 °C in 15 min. The nanocomposites were washed for 5 min in ethanol.

Transmission Electron Microscopy. Microscopy was performed on a FEI TECNAI G2 F20 X-TWIN TEM using a high-angle annular dark field detector (HAADF). HAADF images were obtained with a 2 Å resolution. High resolution transmission electron microscopy (HRTEM) was performed using a JEOL 2010F TEM operating at 200 kV. Pictures were obtained at the optimum defocus condition. Nanocomposites were deposited from a dilute ethanol solution onto 200 mesh carbon-coated copper TEM grids

X-ray Diffraction. Wide angle X-ray diffraction was performed with samples on a quartz slide using a Bruker-Nonius D8 Advance diffractometer. Samples were typically scanned for 12 h at a scan rate of 12 deg/min with 0.02 deg increments. The average nanocrystal size was estimated from the Scherrer equation by fitting the XRD line shapes using JADE software (by Molecular Diffraction Inc.).

Catalysis. 1-decene hydrogenation reactions were carried out in a 25 mL round-bottom flask batch reactor as reported previously.[22] Supported FePt nanocrystals were added to neat 1-decene to create a 2000:1 decene to iridium mass ratio. Reaction conversion was identified using GC-MS.

Results

Structure of Nanocomposites after Infusion of FePt Nanocrystals. Figure 1 shows a representative high-resolution TEM of FePt of the original nanocrystals prior to infusion, along with a histogram of the particle number distribution. The particles are spherical in shape and crystalline as can be seen from the lattice fringes in HRTEM. The lattice spacing is estimated to be 2.24 Å, which matches to the (111) plane as reported by Sun.[38] Upon counting 250 particles, the average diameter was found to be 3.6 ± 0.5 nm as shown in the histogram. The mesoporous silica as synthesized is of type SBA-15 with hexagonally ordered 1D cylindrical mesopores. The mesoporous silica had a surface area of 540 m^2/g, a mean pore diameter of 5.5 nm, and a wall thickness of 4.3 nm (see Figures S2 and S3 in the Supporting Information).

The presynthesized FePt nanocrystals were infused into the mesoporous silica for 10 min. Figure 2 shows the loadings reached 14 wt % as a function of initial nanocrystal concentration in toluene. The loading markedly exceeds previous values which was a maximum of 2.5 wt % using sc-CO$_2$ as an antisolvent.[14] The loadings may be tuned linearly as a function of the initial FePt concentration. At low initial concentrations (∼0.25 mg/ml), nearly all of the FePt nanocrystals in the bulk were adsorbed within the mesoporous silica, leaving a clear supernatant. At a higher initial concentration of 2 mg/mL, the final concentration of nanocrystals after infusion was only ∼0.37 mg/ml in the supernatant, indicating that more than 3/4 of the original nanocrystals were adsorbed. The loadings for FePt nanocrystals were measured as a function of time to determine the kinetics of nanocrystal infusion (see the Supporting Information, Table 1). For an initial concentration of 0.7 mg/mL, loadings increased from 8.9 to 11.4 wt % when the time of infusion was increased from 10 min to 16 h, suggesting an approach to equilibrium. For higher initial concentrations of 2 mg/mL, the loadings increased slightly from 13.8 wt %

(45) Zhao, D.; Huo, Q.; Feng, J.; Chmelka, B. F.; Stucky, G. D. *J. Am. Chem. Soc.* **1998**, *120*, 6024–6036.
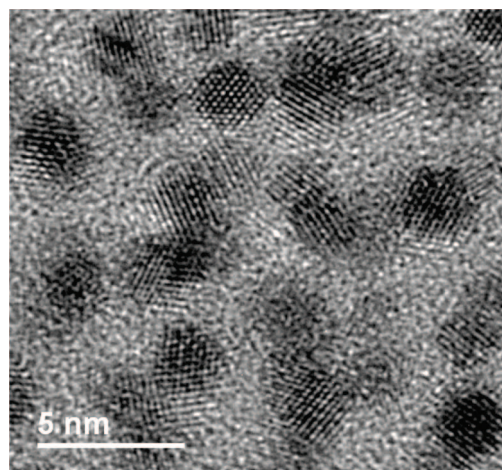
(a)
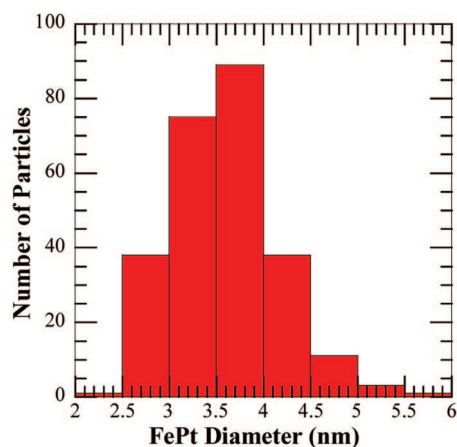
(b)

Figure 1. (a) HRTEM images of presynthesized FePt nanocrystals prior to infusion. (b) Histogram of nanocrystal size. Average diameter is 3.6 ± 0.5 nm; 250 nanocrystals were counted for the histogram.
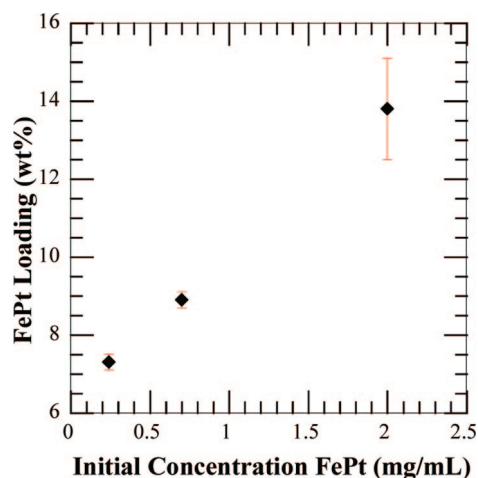

Figure 2. Loading of FePt nanocrystals within mesoporous silica in 10 min as a function of initial concentration of nanocrystals.

to 14.3 wt % over this time interval, which is within the experimental reproducibility. Thus, the level of loading approached a near equilibrium value on the order of minutes.

High-resolution HAADF-STEM was used to visualize the FePt nanocrystals supported on the mesoporous silica prior to thermal annealing. The contrast variation is proportional to the mass density of the region multiplied by the atomic

number Z squared.[34] Regions of high atomic number appear in white. The image of the system may be understood as a convolution of the probe, the SiO_2 support and the metal nanocrystals.

$$I(\text{total}) = I_{\text{probe}} \theta I_M \theta I_{SiO2} \qquad (1)$$

where the symbol θ represents the convolution operation. The interpretation of the image can be complicated. However the SiO_2 porous structure is periodic and relatively straight-forward to understand and allows the interpretation of the HAADF images. On the other hand, the particles are located in both black and white fringes, with somewhat similar sizes in each domain. Figure 3a shows a planar view of the FePt nanocrystals aligned within the pores at 7.3 wt % metal loading after infusion. FePt nanocrystals are observed as spherical bright dots, silica walls appear as white lines and empty pores appear as dark spaces between the silica walls, as expected because of differences in atomic number. The nanocrystals are highly dispersed without any significant aggregation. The FePt nanocrystals associated more with the dark line regions are more likely to be in the pores and are estimated to be 65% of the total infused nanocrystals, whereas those in the white regions can be either on the surface or in the pore just above or below the pore wall or in the secondary interconnecting pores.[21] The secondary pores of size up to 3.6 nm are present in SBA-15 mesoporous silica as reported by Joo and Ryoo.[21] Most of the nanoc-rystals are aligned with the pores along the pore wall and show a definite orientation parallel to the pores, suggesting that they are in the pores, and not the external surface. In addition, many of the particles in the white domains are also in the pores. The FePt nanocrystals in the tail end of the distribution with 5 nm metal cores (and 1.8 nm long ligands on the metal surface) will not be able to enter the pores with a diameter of 5.5 nm. These larger nanocrystals may only be adsorbed on the external surface and appear in the white regions of the pore walls. As a result, the average size of some of the nanocrystals that appear on the white lines or pore walls is larger (>4 nm) than that of the nanocrystals in the dark spaces or pores (~3.5 nm).

The average interparticle distance between the nanocrystals in Figure 3a is between 5 and 10 nm. Assuming a uniform distribution of nanocrystals for a 7.3 wt % loading in the cylindrical mesopores, the average interparticle distance was estimated to be 35 nm. The STEM micrograph is necessarily obtained near an edge of a particle where the particle is not too thick. Thus, this difference in interparticle distance suggests that nanocrystals are more concentrated closer to the pore openings than in the center of the pore, as they have to diffuse longer distances to reach the center of the pore. The bright-field high-resolution image of the FePt nanoc-rystals in Figure 3b indicates that the nanocrystals retain their size and crystallinity as confirmed by the presence of lattice fringes. The lattice spacing of these supported FePt was estimated to be 2.28 Å, which is comparable to the value of 2.24 Å (for (111) plane) estimated for unsupported nanocrystals.
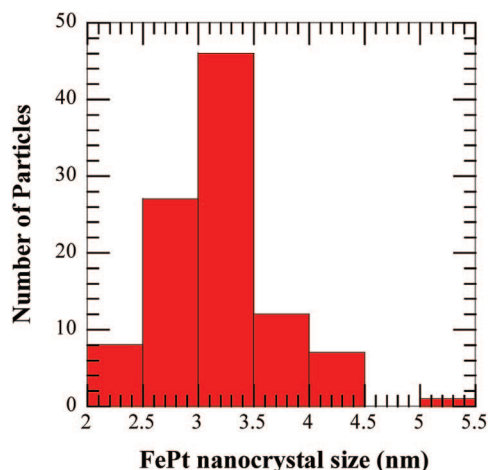
A calculation of the surface coverage of the nanocrystals may be used to provide further evidence that the nanocrystals are in the pores and not merely adsorbed on the external surface. The external surface area of mesoporous silica is extremely small, ~0.3 m²/g on the basis of a particle size
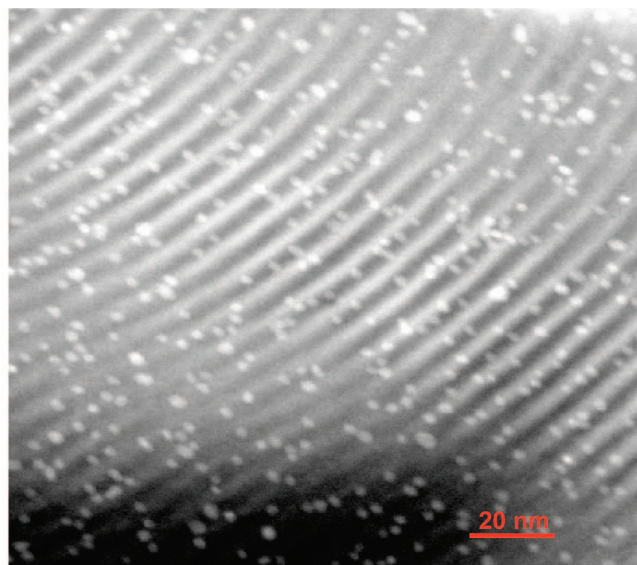
(a)
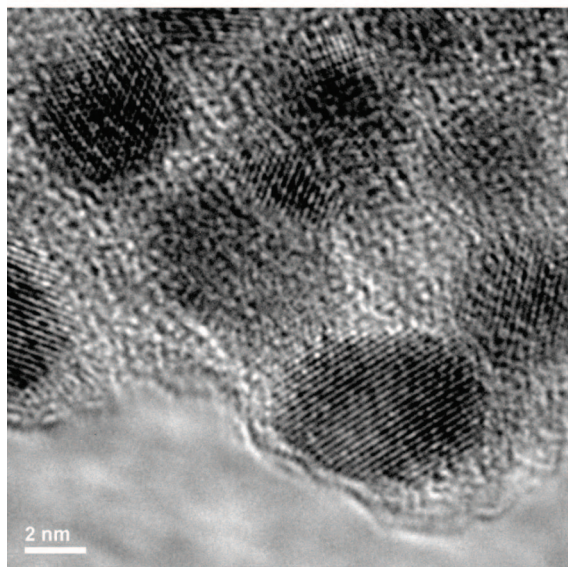
(b)

(c)

Figure 3. TEM images of 7.3 wt % FePt nanocrystals after infusion into mesoporous silica. (a) HAADF STEM planar view; (b) HRTEM; (c) histogram of nanocrystal size using (a) for 100 nanocrystals.
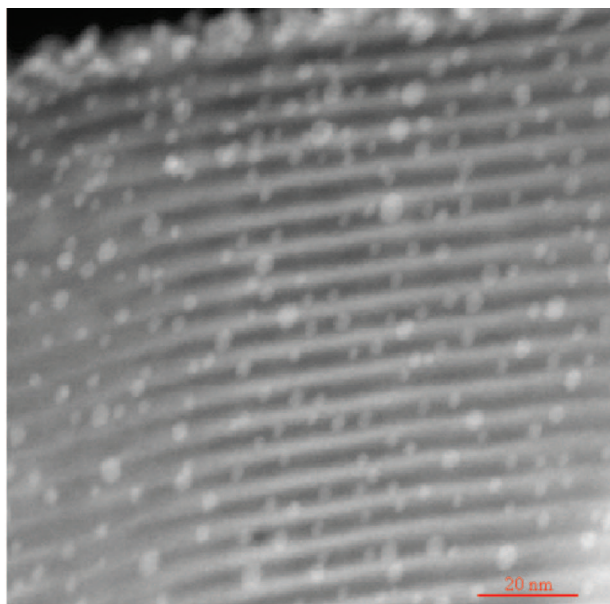
estimate of 10 μm. For an area/particle of 1.57×10^{-10} m^2 on the surface, a closely packed monolayer of FePt nanoc-

rystals would only produce a loading of < 0.5 wt %. The observed loading of 10 wt % would require at least 20 layers of nanocrystals, if all the particles were located on the external surface. As can be seen in Figure 4a, the thickness of the nanocrystal layer on the external surface is only a few layers thick, far below 20. Thus, the STEM-HAADF images and this calculation suggest that most of the particles were adsorbed in the mesopores and not on the surface.
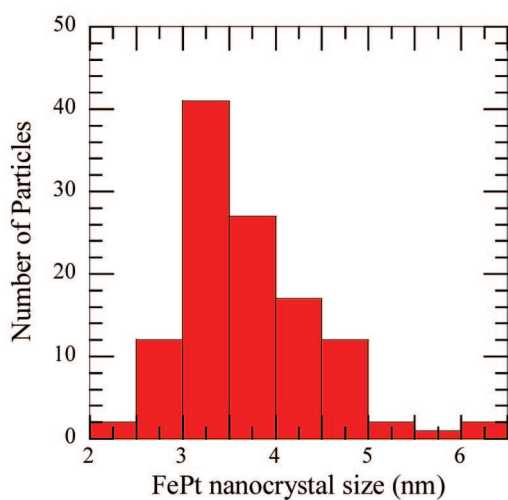
Stability of the Nanocrystals on the Support against Desorption and Sintering. The stability of the supported FePt nanocrystals toward desorption in polar and nonpolar solvents was studied in ethanol and toluene separately. Twenty milligrams of 7.3 wt % FePt in mesoporous silica was dispersed in 5 mL of solvent and sonicated for 2 h at ambient temperature. Using UV−vis spectroscopy, the absorbance was less than 0.01. Thus, a maximum of less than 2.5% of the total infused nanocrystals for both solvents could have desorbed, a very minor amount, within the error limit of the instrument.

The stability of supported FePt nanocrystals toward sintering and coalescence at high temperature was character-ized by annealing the nanocomposite at 700 °C as shown in the STEM-HAADF images in Figure 4a. Most of the nanocrystals are well-dispersed without any noticeable ag-gregation. From the TEM image in Figure 4a, pore collapse or structural damage is not present for the mesoporous silica thermally treated at 700 °C. The size of the larger nanoc-rystals in the distribution is still within the range of the as synthesized nanocrystal dispersion shown in Figure 3c. The size distribution of annealed supported nanocrystals as seen in the histogram (Figure 4b) was very similar to that of as-synthesized nanocrystals prior to infusion. However, there are a few regions in the STEM image that show sintering of nanocrystals, as examined in greater detail in the Supporting Information, Figure S4. These regions are likely on the external surface of the silica and not within the pores.
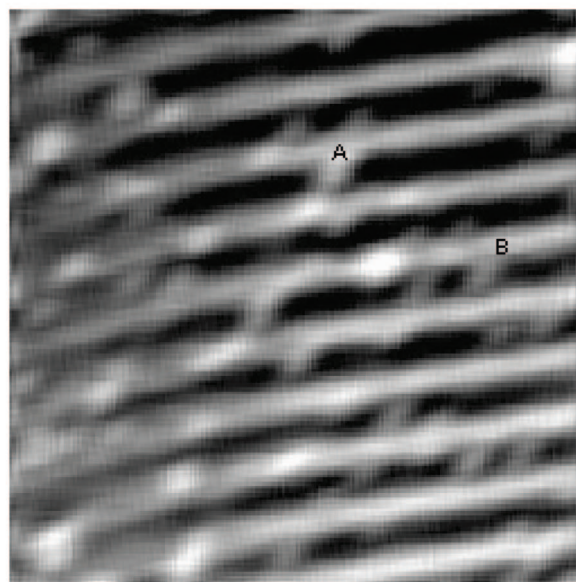
The STEM image in Figure 4a was filtered to eliminate shot noise, as shown in Figure 4c. Because of the fact that most of the particles are of the same composition, the STEM-HAADF profile represents the profile of the size and shape of the nanocrystals. The intensity profile of larger particles in region A (Figure 4d) can be compared with the smaller particles in region B (Figure 4e). The particles in A are more intense and are less spherical than the particles in B. The size of the particles in A approaches the pore size of 5 nm. Therefore, it is reasonable to assume that the particles in A wetted the external surface of the silica during thermal annealing. Figure 4d shows two small nanocrystals near each other. In contrast with the large type A particles, the size of the type B nanocrystals is ∼3 nm, well-below the pore size. If the B particles were on the surface of the silica, it is likely that the particle would sinter at the high annealing temper-ature. Thus, it is likely that the B particle was in a pore. From a statistical analysis of the number of particles of type A and B in a sample of 106 nanocrystals, 85 correspond to type B, based on a size cutoff of 4.5 nm. With the STEM analysis of the samples before and after calcination, along with the calculation of the particle surface coverage, it is evident a large fraction (at least 80%, a conservative estimate)
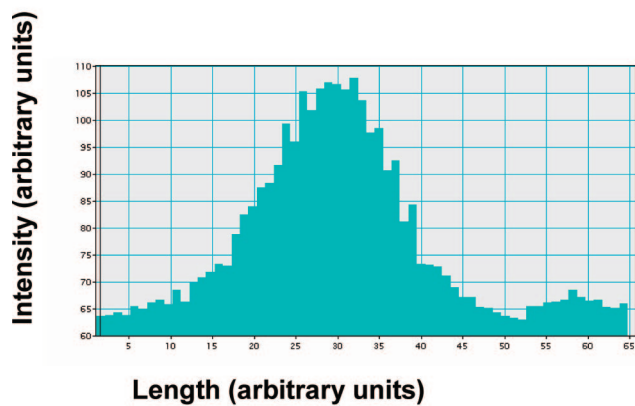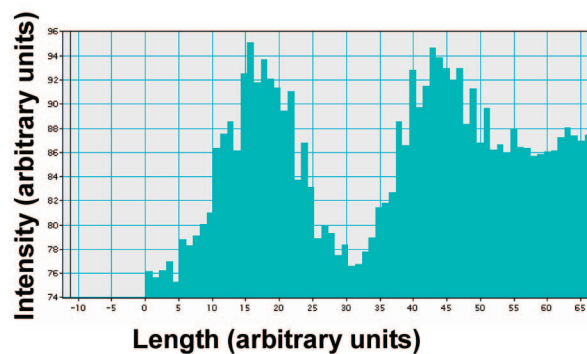
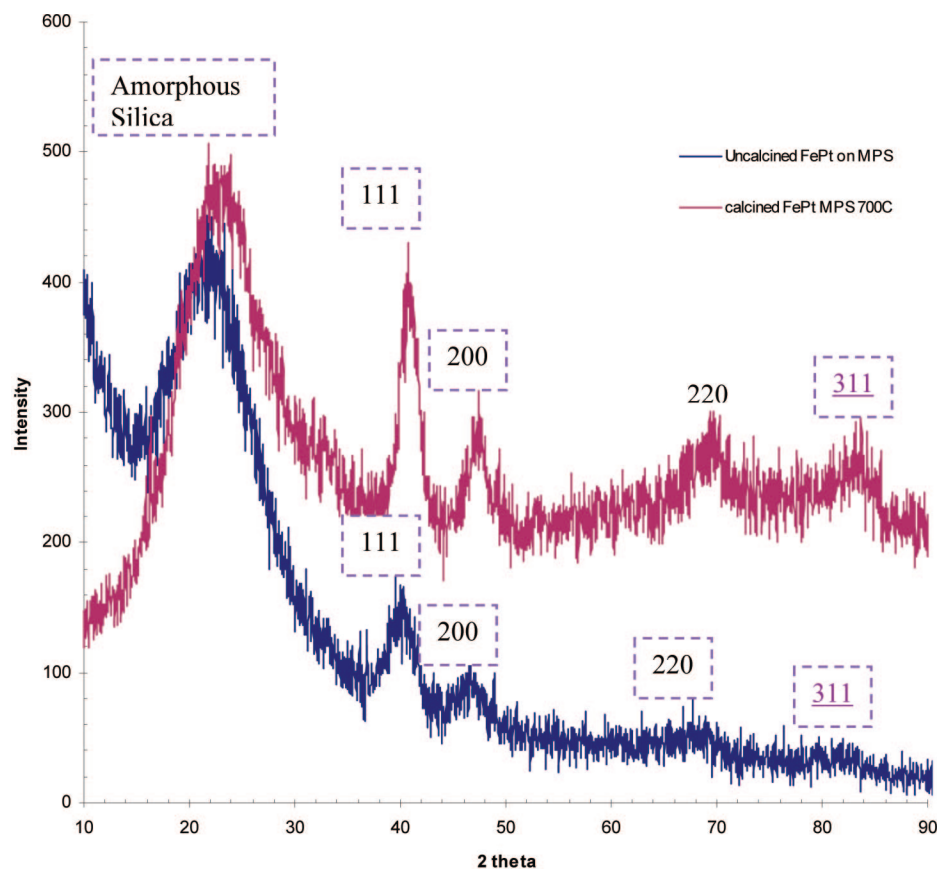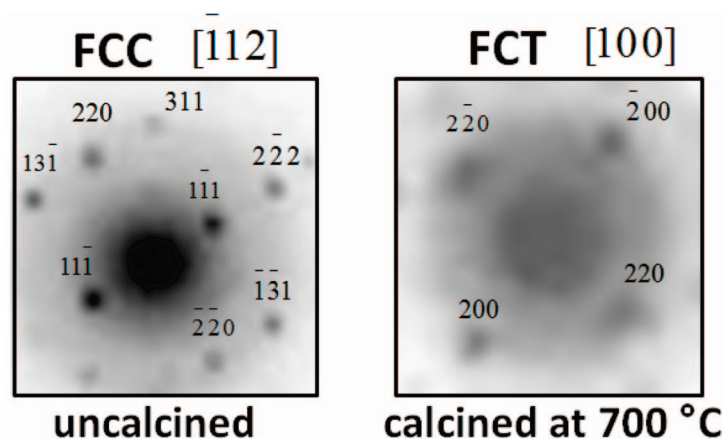**Figure 4.** 7.3 wt % FePt nanocrystals in mesoporous silica calcined at 700 °C for 4 h: (a) HAADF- STEM. (b) Histogram of nanocrystals after calcination determined from (a). 116 nanocrystals were counted. Average size is 3.7 ± 0.7 nm. (c) Filtered image of random portion of (a) to eliminate shot noise. (d) Intensity profile of FePt marked (A) in image (c). (e) Intensity profile of FePt marked (B) in image (c).

Figure 5. (a) XRD diffraction of 7.3 wt % FePt nanocrystals in mesoporous silica before and after annealing at 700 °C. The (111) peak to the right shift after annealing at 700 °C supports the phase transition from FCC phase of uncalcined nanocrystals to FCT (L1$_0$). (b) Convergent beam electron diffraction of 7.3 wt % FePt nanocrystals in mesoporous silica before and after annealing also confirms phase transformation from FCC to FCT phase.

of the particles was in the pores. Furthermore, nanoparticles on the external surface will sinter on annealing as shown in the Supporting Information, Figure S4, and on the top edge of the Figure 4a. The small degree of sintering shown in STEM images and in the XRD results indicate that a large fraction of the particles were protected in the pores.

Crystal Structure of the Bimetallic FePt After Annealing. To facilitate the ordering of atoms in the supported FePt nanocrystals, we annealed the samples at 700 °C. The change in crystal structure of FePt nanocrystals on

thermal annealing was observed with wide-angle XRD and convergent beam electron diffraction (CBED) studies. Figure 5a gives the XRD patterns of infused FePt nanocrystals in mesoporous silica, before and after thermal annealing. In the as-synthesized uncalcined nanocomposite, peaks are observed at $2\theta = 40.2, 46.7, 67.6$ and 83° are assignable to the (111), (200), (220), and (311) orientations for FePt. A broad peak is found at $2\theta = 22.5°$, which can be assigned to amorphous silica. The FePt peaks can be indexed to a FCC phase, which is reported to be a disordered phase.[38] From the XRD spectra

according to the Scherrer equation, the nanocrystal size is estimated to be 4.0 nm and is in close agreement with the FePt particle size before infusion measured using TEM. The small nanoparticle sizes lead to weaker and broader peaks than for larger particles.

The XRD spectra for the annealed FePt nanocomposite indicates a (111) peak shift by 0.5°.[38] The full width at half-maximum of the (111) peak of annealed FePt nanocomposite does not show any significant narrowing, as compared to the as-synthesized sample, indicating coalescence of nanocrystals was insignificant, consistent with the STEM results. The nanocrystal size after sintering from peak fitting was ~4.1 nm, close to uncalcined nanocrystal size. Hence, the FePt nanocrystals underwent ordering to the FCT phase upon thermal annealing without any appreciable sintering. The (110) peak for FCT phase is very broad and weak but we used another technique of convergent beam electron diffraction to further study the phase transformation.

The technique of convergent beam electron diffraction (CBED) was employed to confirm the structural changes of nanocrystals loaded in the silica. This is an accurate method to determine three-dimensional information about the reciprocal lattice point and space group symmetry details, lattice parameters from fine regions, and atomic positions within a unit cell.[46,47] Electron diffraction patterns recorded from a single supported FePt nanocrystal are shown in Figure 5b. The patterns are indexed for the single nanocrystal before and after thermal treatment at 700 °C, to identify the change in crystal structure. CBED of a single uncalcined FePt nanocrystal supported on mesoporous silica confirms the FCC phase of the nanocrystals undergoes a phase transformation to FCT phase upon thermal annealing (Figure 5b).

Activity and Stability of Catalysts for 1-Decene Hydrogenation. The turnover frequency (TOF) for the FePt supported on mesoporous silica, calculated from moles of 1-decene reacted per second per mole of active sites on the nanocrystal surface, as described earlier,[22] is shown in Figure 6. The blank mesoporous silica did not have any catalytic effect for decene hydrogenation. Conversion for 1-decene by blank silica was <1% after 4 h (wt of decene: wt of silica = 10:1), and is within the error limits of the GC-MS. The number of active sites for FePt was calculated for a particle size of 3.6 nm, as determined from TEM in Figure 3a. To ensure complete ligand removal, the catalyst was calcined at 500 °C. The temperature was much higher (~100 °C) than where the ligands are removed, as determined by TGA.[48] The reaction was carried out in neat 1-decene. It was zero order with respect to decene and with a linear conversion in time. A large increase in catalyst activity for fresh FePt catalyst was observed after thermal oxidation. To test the stability of the FePt catalyst, it was recovered and used for two more successive reactions. The TOF doubled in the second hydrogenation reaction to a high level of 30 s⁻¹,

(46) Williams, D. B.; Carter, C. B. *Transmission Electron Microscopy*; Springer: New York, 1996.
(47) Ferrer, D.; Torres-Castro, A.; Gao, X.; Sepulveda-Guzman, S.; Ortiz-Mendez, U.; Jose-Yacaman, M. *Nano Lett.* **2007**, *7*, 1701–1705.
(48) Zhang, L.; He, R.; Gu, H.-C. *Appl. Surf. Sci.* **2006**, *253*, 2611–2617.
(49) Shevchenko, E. V.; Talapin, D. V.; Kotov, N. A.; O'Brien, S.; Murray, C. B. *Nature* **2006**, *439*, 55–59.
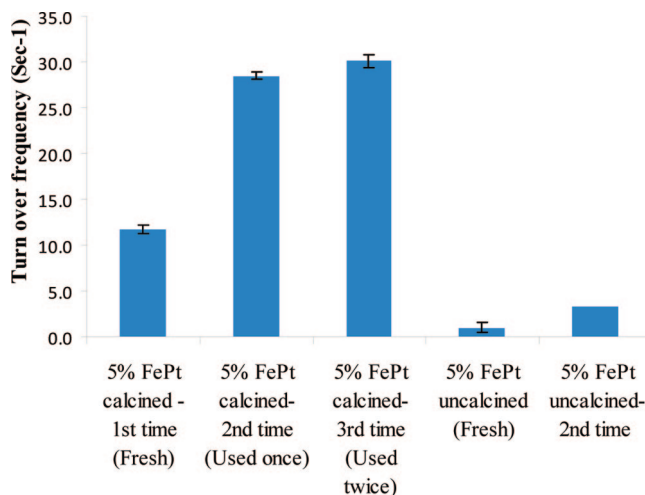
Figure 6. Turnover frequency for 1-decene hydrogenation by 5 wt % FePt in mesoporous silica.

which is twice that observed for the 4.5 nm iridium catalyst,[22] and did not show any significant increase for the third reaction. The corresponding specific activity was 8.5×10^{-4} mol g⁻¹ s⁻¹, which was 6 times higher than the industrial catalyst 5 wt % Pd-alumina; however, the metals were different in each case. As the size of the Pd nanoparticles is not known, TOF for Pd-alumina cannot be calculated. The uncalcined as synthesized FePt nanocomposite exhibited significant catalyst activity (~33% relative to a 5% Pd-alumina industrial catalyst). Thus, the passivating ligands did not block the entire metal surface. The reproducibility in the TOFs was determined by synthesizing new batch of 5% FePt-silica catalyst and then repeating the reactions (fresh, washed once, and washed a second time). The reprodubility for all cases was within 5% of the 1-decene conversion and is within the detection error of GC-MS. During infusion, the weakly bound ligands may desorb and adsorb on the silica with a much larger surface area.[22] The catalyst activity doubled relative to the first reaction when the uncalcined FePt nanocomposites were used for a second reaction. The performance of the FePt catalyst after the first cycle was three times better than the commercial catalyst (5% Pt on alumina). The significant increase in the activity of the calcined catalyst for the second run may likely be attributed to the removal of carbonaceous contaminants that block active sites from the metal surface. The lack of change during the third run suggested that these contaminants were completely removed.

Discussion

Effect of Specific Short- And Long-Range Metal−support Interactions on the Metal Loading and Stability. The inherent stability of the nanocrystals against desorption into polar solvents at low temperature or sintering at 700 °C may be attributed to two key factors, electronic and geometrical effects. Zheng and Stucky have reported that gold nanocrystals stabilized with thiol ligands adsorbed on nonporous substrates, such as silica and titania, adsorb weakly and desorb readily into a polar solvent such as ethanol.[7]

Metal−support interactions play a key role in both the activity and the thermal stability of the nanocrystal catalysts. Yu et al. studied the thermal stability of Pt nanocrystals supported on silica thin films using in situ TEM.[44] The particles began to change shape at 350 °C, and spread on the surface above 500 °C. The wetting of the surface by the nanocrystals is attributed to the interfacial mixing of Pt and silica, as a result of strong metal−support interactions. Klie et al. characterized Pt-silica specific short-range interactions using electron energy loss spectroscopy.[43] Strong silica charge transfer interactions with Pt were identified using X-ray photoelectron spectroscopy (XPS).[42] Similar strong interactions between Pt atoms on the surface of FePt nanocrystals and silica may be expected to aid both the infusion process and the stabilization of the particles upon thermal annealing.

Long-ranged electrostatic and van der Waals interactions also contribute to the interaction between a nanoparticle and the support. FePt nanocrystals did not did not migrate under a field of 166 V/cm, indicating minimal charging. Silica in nonpolar media acquires negative charges[50] but the surface charge density is very small, with each charge separated by ∼100 nm. Metal nanoparticles are extremely polarizable and form a large induced dipole in presence of a charge.[51] The attractive charge-induced dipole interactions between charged silica and a single metal nanocrystal (see the Supporting Information, Figure S5) are proportional to the cube of the nanocrystal radius, whereas the long-ranged van der Waals interactions were found to be weakly repulsive in toluene. The total long-ranged interaction energy (charge-induced dipole + van der Waals) is only weakly attractive for the 3.6 nm FePt nanocrystals (see Figure S5 in the Supporting Information). However, with the sparse charge densities for silica (20−200 charges/μm^2) the total loading would be only 0.5 wt % if one nanocrystal interacted with each charge on the silica. Consistent with this prediction, we have shown that 2 nm gold nanocrystals stabilized by dodecanethiol adsorb weakly on silica with small loadings of < 0.3 wt %.[22] Therefore, the high levels of adsorption for both the FePt and Pt nanocrystals (up to 20%) in this study must be driven primarily by the short-ranged interactions described above.[42–44]

The hydrocarbon capping ligands on the metal surface must not screen the strong short-ranged interactions with the silica. Amines and fatty acids are known to bind to Au more weakly relative to thiols.[52] For example, surface coverage of dodecylamine on Pt is 46%[53] compared to 75% for dodecanethiol on Ag.[54] The lower surface coverage exposes more bare metal surface for the formation of specific short-ranged interactions with the silica. These short-ranged interactions could explain the loadings of ∼20 wt %, relative to the much lower loadings for gold capped with dode-

canethiol, where the surface coverage is higher. Furthermore, more of the weakly bound amine ligands will migrate from the nanocrystals to the silica surface and expose even more surface area than in the case of the strongly bound thiols. The large thermodynamic driving force for adsorption in the FePt case led to near equilibrium loadings in only 10 min versus 24 h for the dodecanethiol capped gold.[22] The short-ranged specific interactions were sufficient to prevent sintering from mobilization of nanocrystals at high temperatures up to 700 °C and from desorption into both polar (ethanol) and nonpolar (toluene) solvents upon sonication. The controlled particle size and composition were favored by the metal−support interactions, ease of ligand removal at moderate temperatures (<400 °C) and the removal of byproducts of nanocrystal synthesis prior to infusion. The convex surfaces on the nanocrystals favored contact with the cylindrical mesopores with concave curvature.[55] In contrast, the surfaces of both the metal nanocrystal and support are often both convex for traditional supports leading to a smaller degree of interfacial contact. The beneficial geometrical effect of enhanced interfacial area on nanocomposite stability has been reported by Rolison and co-workers for 1−10 wt% gold-titania composites.[56,57]

Previously, loadings only reached ∼2.5 wt% for gold nanocrystals, coated with strongly bound alkanethiols, infused into silica with CO_2 as an antisolvent in toluene.[14] The addition of CO_2 lowers the Hamaker constant of the intervening solvent and strengthens the van der Waals interactions of the particles with the silica, thus raising the nanocrystal loading.[14] In the present study, it was not necessary to add CO_2 to drive the nanocrystal loadings because the particle−support interactions were strong as a consequence of the weakly bound ligands.

Design of Bimetallic Nanocrystals. The results in Figures 1, 3, and 5 indicate that the size, composition, and crystal structure of the bimetallic nanocrystals were relatively uniform. These properties may be shown to be favored by the arrested precipitation in the presence of stabilizing ligands.[61,62] Here, the dynamic solvation of the nanocrystal surface by the ligands may be tuned to produce regions of the nanocrystal surface accessible for growth, while providing enough steric repulsion to inhibit nanocrystal aggregation. The temperature may be varied to adjust the precursor decomposition and consequently the supersaturation, nucleation and growth rates. At sufficiently high temperature and monomer concentrations, the balance between interfacial energy and supersaturation produces a small critical size where the growth rate is zero.[62] Here, the nanocrystal diameter may be focused to narrow polydispersity, as seen

(50) Papirer, E. *Adsorption on Silica Surfaces*; CRC Press: Boca Raton, FL, 2000; Vol. 90.
(51) Israelachvili, J. *Intermolecular & Surface Forces*, 2nd ed.; Academic Press: San Diego, 1992.
(52) Jana, N. R.; Peng, X. *J. Am. Chem. Soc.* **2003**, *125*, 14280–14281.
(53) Fu, X.; Wang, Y.; Wu, N.; Gui, L.; Tang, Y. *J. Colloid Interface Sci.* **2001**, *243*, 326–330.
(54) Korgel, B. A.; Fullam, S.; Connolly, S.; Fitzmaurice, D. *J. Phys. Chem. B* **1998**, *102*, 8379–8388.
(55) Haller, G. L. *J. Catal.* **2003**, *216*, 12–22.
(56) Pietron, J. J.; Stroud, R. M.; Rolison, D. R. *Nano Lett.* **2002**, *2*, 545–549.
(57) Rolison, D. R. *Science* **2003**, *299*, 1698–1702.
(58) Shah, P. S.; Holmes, J. D.; Doty, R. C.; Johnston, K. P.; Korgel, B. A. *J. Am. Chem. Soc.* **2000**, *122*, 4245–4246.
(59) Shah, P. S.; Husain, S.; Johnston, K. P.; Korgel, B. A. *J. Phys. Chem. B* **2001**, *105*, 9433–9440.
(60) Shah, P. S.; Husain, S.; Johnston, K. P.; Korgel, B. A. *J. Phys. Chem. B* **2002**, *106*, 12178–12185.
(61) Brust, M.; Walker, M.; Bethell, D.; Schiffrin, D. J.; Whyman, R. *J. Chem. Soc., Chem. Commun.* **1994**, *7*, 801–802.
(62) Yin, Y.; Alivisatos, A. P. *Nature* **2005**, *437*, 664–670.

in Figure 1, as the growth rate is higher for the smaller nanocrystals than the larger ones.[62] The focusing is optimal if the monomer concentration and dynamic solvation maintain the average nanocrystal size slightly larger than the critical size.

A variety of previous studies indicate that the size and composition of bimetallic nanocrystals may be controlled over a significant range in the arrested precipitation technique by varying the temperature and precursor concentrations.[38,40,63–66] When the rates of precursor decomposition and equilibrium solubilities of the two resulting metals are similar, formation of binary metal nuclei is favored.[40] Even when these properties are somewhat dissimilar, the nuclei formed from the first metal may capture newly formed atoms of the second metal before it nucleates, which would otherwise lead to two separate populations of growing nanocrystals.[39] In essence, this may be considered to be composition focusing by analogy to size focusing. As metal from the more rapidly decaying precursor is incorporated into the nanoparticle, it will be depleted in the solution relative to the second metal. Thus, the probability of adding the second component will increase. This process will focus the overall composition as well as the particle size. The temperature is a key variable to produce rapid decomposition of both precursors to achieve focusing of both size and composition, along with sufficient dynamic solvation by the ligand to arrest growth. Because our FePt nanocrystals were presynthesized, heterogeneous sites on a support were not present, which could otherwise lead to uncontrolled composition, resulting from competition between nucleation in solution and on the surface. Once the particles are presynthesized, they may be loaded physically into the pores of the support at completely different concentrations than those used in the synthesis of the particles. Thus, both the presynthesis and infusion steps may be optimized in ways not available when precursors are reduced within pores of the support.

A variety of factors complicate control over the size, composition, and morphology of bimetallic nanocrystals synthesized by the traditional technique of precursor reduction directly on a support.[36] The precursors may be reduced either simultaneously or sequentially.[67–70] The diffusional resistance of the precursors through the pores may prevent the production of large supersaturation values that favor control of nucleation, growth and size focusing. For simultaneous impregnation, the metal ions may separate chromatographically as they diffuse into the pores, leading to large variation in nanocrystal composition.[67] For sequential impregnation, the second metal may form a shell around the

first metal, or even nucleate on separate heterogeneous sites on the support.[68] High-temperature annealing may promote alloying between metals, but can also cause sintering of the nanoparticles.[67] Without the use of stabilizing ligands, dynamic solvation is not present to aid size and composition focusing. The precursor concentrations of the metals must be chosen to control both the particle size and composition, as well as the final metal loadings on the support. For example, low precursor concentrations for low loadings may produce insufficient supersaturation and thus defocusing,[62] whereas high loadings may require long reaction times, which may lead to multiple nucleation events resulting in polydispersity. Another challenge is that the reactants and/or byproducts formed during the reduction step may prevent adhesion of the metal particles on the support, resulting in limited catalyst stability. In the presynthesis technique, the particles may be isolated from unwanted byproducts, cleaned, and separated by size, and the ligands may be exchanged if desired prior to infusion.

Thermal annealing above ∼550 °C may be utilized to order the atoms in the FePt nanocrystals to form an intermetallic alloy.[38] The reduction in the melting point of the nanocrystals can cause spreading of the nanocrystals as they wet the support.[44] The resulting surface diffusion may lead to coalscence.[71] This undesired coalescence appeared to be mitigated with the presynthesized nanocrystals, indicating strong metal−support interactions (Figure 4). Ligand removal at moderate temperatures below the melting point further strengthens interactions between the bare metal and the support.

High-temperature annealing is not always needed to make ordered multimetallic nanocrystals by the "polyol process" Ordered intermetallic nanocrystals have been synthesized in solvents including ethylene glycol[72–74] or tetraethylene glycol[75,76] with a control over the size at 100−300 °C. These ordered nanoparticles may then be infused into the support to form catalysts without the need for high-temperature thermal annealing.

Catalytic Activity of Supported Nanocrystals. FePt catalysts were highly active and stable for 1-decene hydrogenation for at least three reaction cycles. The enhanced stability may be attributed to the strong short-ranged metal−support interactions, which prevent desorption or coalescence/aggregation of the metals during the reaction. For the hydrogenation of 1-hexene, the TOF of bimetallic Pd−Ru nanoparticles exceeded by 10 times that of individual Pd and Ru nanoparticles indicating synergism between these

(63) Sra, A. K.; Ewers, T. D.; Schaak, R. E. *Chem. Mater.* **2005**, *17*, 758–766.

(64) Santiago, E. I.; Varanda, L. C.; Villullas, H. M. *J. Phys. Chem. C* **2007**, *111*, 3146–3151.

(65) Alden, L. R.; Roychowdhury, C.; Matsumoto, F.; Han, D. K.; Zeldovich, V. B.; Abruna, H. D.; DiSalvo, F. J. *Langmuir* **2006**, *22*, 10465–10471.

(66) Sun, S. *Adv. Mater.* **2006**, *18*, 393–403.

(67) Ponec, V.; Bond, G. C. *Catalysis by Metals and Alloys*; Elsevier: Amsterdam, The Netherlands, 1995.

(68) Venezia, A. M.; Liotta, L. F.; Deganello, G.; Schay, Z.; Guczi, L. *J. Catal.* **1999**, *182*, 449–455.

(69) Konopny, L. W.; Juan, A.; Damiani, D. E. *Appl. Catal., B* **1998**, *15*, 115–127.

(70) Batista, J.; Pintar, A.; Gomilsek, J. P.; Kodre, A.; Bornette, F. *Appl. Catal., A* **2001**, *217*, 55–68.

(71) Wang, Z. L.; Petroski, J. M.; Green, T. C.; El-Sayed, M. A. *J. Phys. Chem.B* **1998**, *102*, 6145.

(72) Jeyadevan, B.; Hobo, A.; Urakawa, K.; Chinnasamy, C. N.; Shinoda, K.; Tohji, K. *J. Appl. Phys.* **2003**, *93*, 7574–7576.

(73) Iwaki, T.; Kakihara, Y.; Toda, T.; Abdullah, M.; Okuyama, K. *J. Appl. Phys.* **2003**, *94*, 6807–6811.

(74) Roychowdhury, C.; Matsumoto, F.; Mutolo, P. F.; Abruna, H. D.; DiSalvo, F. J. *Chem. Mater.* **2005**, *17*, 5871–5876.

(75) Minami, R.; Kitamoto, Y.; Chikata, T.; Kato, S. *Electrochim. Acta* **2005**, *51*, 864–866.

(76) Leonard, B. M.; Bhuvanesh, N. S. P.; Schaak, R. E. *J. Am. Chem. Soc.* **2005**, *127*, 7326–7327.

Stable Ordered FePt Si Catalysts with High Loadings

Chem. Mater., Vol. 20, No. 15, 2008 5015

two types of atoms.[77] Similar effects have been reported for other bimetallic catalysts.[78] The uniform composition of the presynthesized bimetallic nanocrystals in the current study and the ability to control the intermetallic alloy structure may be expected to be beneficial for achieving these types of synergistic effects on catalytic activity.

The FePt particle size formed by precursor reduction of 6 nm in mesoporous FePt SBA-15 silica without ligands[32] was much larger than the 3.6 nm particles formed in the current study by infusion of ligand stabilized particles. Furthermore, upon ordering the FePt by thermal annealing at 650 °C, the size increased modestly from 6 to 7.2 nm. As the particles approach the pore size of the silica, blocking of pores may limit mass transfer during catalysis. Furthermore, the surface area/volume is two times larger for our 3.6 nm particles versus 7.2 nm particles.

Reducing the size of the metal nanoparticles below 5 nm significantly increases the fraction of surface atoms and hence the mass catalytic activity. For the small 3.6 nm FePt nanocrystals, the morphologies of the crystal facets may be designed to produce more active surfaces than for large particles.[79] For example, atoms present on the jagged "step edges" of small gold nanoparticles (<5 nm) were found to be highly catalytically active for CO oxidation.[2] Presynthesis of the bimetallic nanocrystals may enable greater control over these types of active sites versus traditional precursor reduction techniques, with the potential of higher catalyst activity and selectivity.

Conclusions

Herein, we have demonstrated a novel method to design highly stable and active catalysts composed of bimetallic nanocrystals on mesoporous supports with a controlled intermetallic alloy structure. The catalysts were formed by infusion of presynthesized nanocrystals with well-controlled size and composition. The arrested growth precipitation favors focusing of the size (<4 nm) as well as the composition of the nanocrystals. The stabilizing ligands control dynamic solvation, supersaturation, nucleation, and growth, as reflected in the small nanocrystal size. The low surface coverage of the weakly bound ligands resulted in strong metal−support interactions,[44] as indicated by high metal loadings above 10 wt % in only 10 min and stability against sintering upon thermal annealing at 700 °C. These interactions are further increased by the enhanced interfacial contact area between the metal nanocrystals and concave mesopores with similar radii. For strongly binding ligands such as dodecanethiol[22] or polymers such as polyvinylpyrrolidone[13] with high surface coverages, high loadings were not achieved. According to HAADF-STEM, more than 80% of the nanocrystals were within the pores, relative to the external surface, consistent with the resistance to sintering at 700 °C. Finally, the calcined FePt catalyst was found to exhibit 6-fold higher catalyst activity than commercial Pd-alumina catalyst for liquid 1-decene hydrogenation and was stable for multiple reactions. The decoupling of nanocrystal synthesis and infusion provides exquisite control of the nanocrystal size, alloy structure, binding to the support, and dispersibility within the pores, relative to conventional precursor reduction techniques. The ability to design catalyst morphology and crystal structure with presynthesized bimetallic nanocrystals offers novel opportunities for enhanced catalyst activities, selectivities, and stabilities.

Supporting Information Available: Additional characterization by nitrogen porosimetry, SAXS, STEM, and long-ranged van der Waals model (PDF). This material is available free of charge via the Internet at http://pubs.acs.org.

CM800879Q

(77) Raja, R.; Hermans, S.; Shephard, D. S.; Johnson, B. F. G.; Raja, R.; Sankar, G.; Bromley, S.; Thomas, J. M. *Chemical Communications (Cambridge)* **1999**, 1571–1572.
(78) Scott, R. W. J.; Sivadinarayana, C.; Wilson, O. M.; Yan, Z.; Goodman, D. W.; Crooks, R. M. *J. Am. Chem. Soc.* **2005**, *127*, 1380–1381.
(79) Cho, A. *Science* **2003**, *299*, 1684–1685.